Rapid Communications   Editors' Suggestion

Second-order Dirac superconductors and magnetic field induced Majorana hinge modes

Sayed Ali Akbar Ghorashi,[1,*] Xiang Hu,[1] Taylor L. Hughes,[2] and Enrico Rossi[1]

[1]*Department of Physics, William & Mary, Williamsburg, Virginia 23187, USA*
[2]*Department of Physics and Institute for Condensed Matter Theory, University of Illinois at Urbana-Champaign, Illinois 61801, USA*

We identify three-dimensional higher-order superconductors characterized by the coexistence of one-dimensional Majorana hinge states and gapless surface states. We show how such superconductors can be obtained starting from the model of a spinful quadrupolar semimetal with two orbitals and adding an s-wave superconducting pairing term. By considering all the possible s-wave pairings satisfying Fermi-Dirac statistics we obtain six different superconducting models. We find that for two of these models a flat band of hinge Majorana states coexist with surface states, and that these models have a nonvanishing quadrupolelike topological invariant. Two of the other models, in the presence of a Zeeman term, exhibit helical and dispersive hinge states localized only at two of the four hinges. We find that these states are protected by combinations of rotation and mirror symmetries, and that the pair of corners exhibiting hinge states switches upon changing the sign of the Zeeman term. Furthermore, we show that these states can be localized to a single hinge with suitable perturbations. The remaining two models retain gapless bulk and surface states that spectroscopically obscure any possible hinge states.

The modern theory of polarization for crystalline insulators [1] has revealed that in crystals a dipole moment can be expressed in terms of Berry phases, and that a finite dipole necessarily implies the presence of boundary charges. The presence of nontrivial Berry phases and boundary states are the hallmarks of topological systems [2], and indeed it is now clear that there is a strong connection between the theory of topological insulators (TIs) and systems with quantized dipole moments [3–5]. This connection has led to the realization that the extension of the modern theory of polarization to higher multipole moments allows the identification of new classes of topological crystalline insulators [6,7], termed "higher-order" TIs (HOTIs). Within this framework, a higher-order multipole TI of order m has a quantized nonzero electric mth pole in the bulk (with $m = 1$ for a dipole, $m = 2$ for a quadrupole,...) and localized charges at its $(d - m)$-dimensional boundaries, d being the insulator's spatial dimension. Since the work of Refs. [6,7], many proposals of HOTIs of various types have been presented [8–12]. Higher-order topological insulating phases have been realized in metamaterial arrays [13–15] and phononic systems [16], and it has been proposed that bismuth [10], strained SnTe [8], and some two-dimensional (2D) transition metal dichalcogenides [17] are second-order TIs. In addition, there has been exciting new work on higher-order topological superconductors (HOTSCs) and topological semimetals (HOTSMs) [9,17–23,25–31].

In this work we identify a class of higher-order topological superconductors: *second-order Dirac superconductors* (Fig. 1). Such three-dimensional (3D) higher-order topological superconductors exhibit the unique property to have both topologically protected Dirac cones for states at the

surface (d-1 boundary) and topologically protected dispersionless Majorana states at the hinges (d-2 boundary). The hinge states can be interpreted as Majorana arcs joining the surface Dirac points. We explicitly show that this unique configuration of surface and hinge states is associated with a topological invariant that can be interpreted as the generalization to the superconducting case of the quadrupole moment. This model can provide a platform to study the interplay of the bulk, surface, and hinge states on an equal footing which can significantly help toward understanding the transport properties of systems with higher-order topology. In addition, we identify 3D superconducting systems that can be driven into a higher-order topological state, exhibiting dispersive helical Majorana states at the hinges, simply via the application of an external magnetic field. Interestingly, we find that the hinges are localized at only two of the four hinges (see [23] and [24] for insulating examples of states localized at two corners). Furthermore, the pairs of corners where the Majorana modes are located can be selected by changing the sign of the magnetic field. We also show that by breaking diagonal/antidiagonal mirror symmetries, it is possible to drive the system into a unique topological state in which Majorana states are present only at one of the hinges.

We start by considering a model for a topological quadrupolar semimetal constructed from layers of 2D quadrupolar topological insulators (TIs) [32]. Schematically, the unit cell for the tight-binding model for the 2D quadrupolar insulator layer is illustrated in Fig. 1(c). For each cell we have two orbitals (c, d) and a spin-1/2 degree of freedom, represented by the four black dots in Fig. 1(c). Let γ_i ($i = x, y$) be the intracell hopping amplitudes [red lines in Fig. 1(c)] and λ_i the intercell hopping [blue lines in Fig. 1(c)]. Hopping processes represented by dotted lines have a phase that is opposite to that of the hopping processes represented by solid
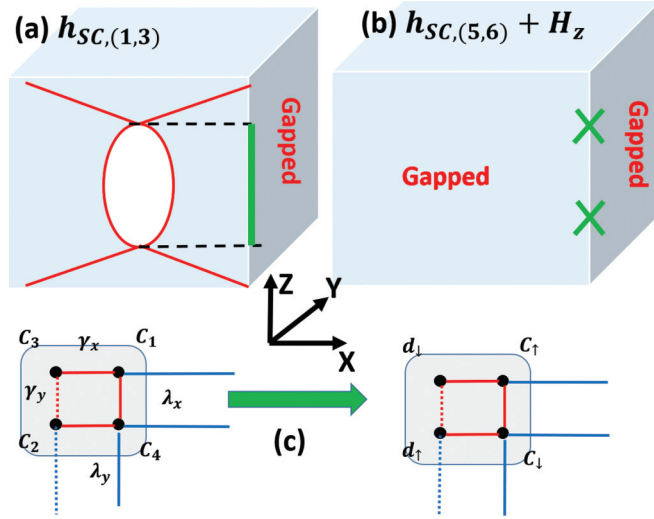
*sghorashi@wm.edu

FIG. 1. Summary illustration of the models with hinge modes studied in this work. (a) Model $h_{SC,1}$ (rotate by C_4 for model $h_{SC,3}$). (b) Models $h_{SC,5}$, $h_{SC,6}$ with magnetic field (Zeeman term H_z) in the z direction. Red lines represent surface states for $k_{x,y} = 0$ cuts. Green lines represent flat-band hinge states; green crosses represent dispersing hinge nodes. (c) The unit cell convention used to convert between spinless and spinful versions of HOTI and HOTSM.

TABLE I. The pairings for the six different models discussed in this work. Columns 2–4 show the representation of the pairing term and of the symmetry operators for each model. $m_x = \sigma_1\kappa_3$, $m_y = \sigma_1\kappa_1$, $\hat{r}_4 = \frac{i}{2}(\sigma_1 + i\sigma_2)\kappa_2 + \frac{1}{2}(\sigma_1 - i\sigma_2)\kappa_0$. Column 6 shows the pairing structure: inter/intra and S/T are short for inter/intra orbital and spin singlet/triplet, respectively. Column 7 shows whether the model is a HOTSC: models with an "*" in parentheses denotes the existence of HOTSC in the presence of magnetic field.

Model	Λ_i	$\mathcal{M}_x$	$\mathcal{M}_y$	$\mathcal{C}_4$	Structure	HOTSC
$h_{SC,1}$	$\sigma_1\kappa_2$	$\tau_3 m_x$	$\tau_3 m_y$		intra-S	✓
$h_{SC,2}$	$\sigma_2\kappa_1$	$\tau_0 m_x$	$\tau_3 m_y$		intra-S	✓
$h_{SC,3}$	$\sigma_2\kappa_0$	$\tau_3 m_x$	$\tau_3 m_y$		inter-S	✓
$h_{SC,4}$	$\sigma_2\kappa_3$	$\tau_3 m_x$	$\tau_0 m_y$		inter-T	✓
$h_{SC,5}$	$\sigma_0\kappa_2$	$\tau_3 m_x$	$\tau_3 m_y$	$\tau_0 \hat{r}_4$	inter-S	$-(\checkmark^*)$
$h_{SC,6}$	$\sigma_3\kappa_2$	$\tau_0 m_x$	$\tau_0 m_y$	$\tau_3 \hat{r}_4$	intra-T	$-(\checkmark^*)$

lines. Depending on the choice of interlayer tunneling terms between 2D layers of quadrupolar TIs we obtain different Hamiltonians, H, for the resulting 3D system. In momentum space we have $H_{SM} = \sum_{\mathbf{k}} \psi_{\mathbf{k}}^\dagger h_{SM}(\mathbf{k})\psi_{\mathbf{k}}$, where $\psi_{\mathbf{k}}^T$ is the spinor $(c_{\mathbf{k}\uparrow}, d_{\mathbf{k}\uparrow}, d_{\mathbf{k}\downarrow}, c_{\mathbf{k}\downarrow})$, formed by the annihilation operators $c_{\mathbf{k}\alpha}, d_{\mathbf{k}\alpha}$, for an electron in orbitals c, d, with spin α and momentum $\mathbf{k}$, and h_{SM} is a 4×4 Bloch Hamiltonian matrix of the general form:

$$h_{SM}(\mathbf{k}) = [\gamma_x + \chi_x(k_z) + \lambda_x \cos(k_x)]\Gamma_4 + \lambda_x \sin(k_x)\Gamma_3$$
$$+ [\gamma_y + \chi_y(k_z) + \lambda_y \cos(k_y)]\Gamma_2 + \lambda_y \sin(k_y)\Gamma_1.$$
$$(1)$$

In Eq. (1) all the lattice constants are taken to be 1, $\chi_i(k_z)$ ($i = x, y$) are periodic functions of k_z with forms fixed by the interlayer tunneling terms, and $\{\Gamma_\alpha\}$ are the 4×4 matrices given by the direct product of 2×2 Pauli matrices σ_i, κ_i in spin and orbital space, respectively: $\Gamma_0 = \sigma_3\kappa_0$, $\Gamma_i = -\sigma_2\kappa_i$, $\Gamma_4 = \sigma_1\kappa_0$. In the remainder we assume $\chi_i(k_z)$, γ_i, λ_i to be independent of the in-plane direction (x or y) such that the normal state topological quadrupolar semimetal has C_4 symmetry. To be explicit we will set $\lambda_i = \lambda$ and use it as our unit of energy with $\lambda = 1$. We then set $\chi_i(k_z) = \cos(k_z)/2$, and $\gamma_i = \gamma = -3/4$. With this choice of parametrization, $h_{SM}(\mathbf{k})$ has fixed k_z "momentum slices" with a nonvanishing quantized quadrupole moment for $\cos(k_z) < -1/2$, and vanishing quadrupole for $\cos(k_z) > -1/2$. As a consequence, the bulk bands are semimetallic with fourfold degenerate nodes at the locations $k_z^{(c)}$ where the quadrupole changes, i.e., $\cos(k_z^{(c)}) = -1/2$ [32]. It is important to point out that any HOTSM with a well-defined nontrivial quadrupole moment and C_4 and mirror symmetries should lead, in the presence of s-wave superconducting pairing, to results qualitatively similar to the one that we present below. The presence of the C_4 and mirror

symmetries is important, as we will show, to be able to "tune" the hinge states via external magnetic fields.

The most general mean-field Hamiltonian describing a superconducting state for our system is given by $H_{SC} = \sum_{\mathbf{k}} \Psi_{\mathbf{k}}^\dagger h_{SC}(\mathbf{k})\Psi_{\mathbf{k}}$ where $\Psi_{\mathbf{k}}^T = (\psi_{\mathbf{k}}, \psi_{-\mathbf{k}}^\dagger)$ is the spinor in Nambu space and $h_{SC}(\mathbf{k}) = \tau_3[h_{SM}(\mathbf{k}) - \mu] + \Delta_0^{(ij)}(\mathbf{k})\tau_2\sigma_i\kappa_j$, where μ is the chemical potential, $\Delta_0^{(ij)}(\mathbf{k})$ the superconducting pairing strength in the (ij) spin-orbital channel, and $\{\tau_i\}$ are the Pauli matrices in Nambu space. Restricting the superconducting pairing to be s-wave, i.e., $\Delta_0^{(ij)}(\mathbf{k}) = \text{const} = \Delta_0$, we obtain

$$h_{SC,i} = \tau_3[h_{SM}(\mathbf{k}) - \mu] - \Delta_0\tau_2\Lambda_i, \qquad (2)$$

where Λ_i is a 4×4 matrix, independent of $\mathbf{k}$, that determines the structure of the superconducting pairing in orbital and spin space. The requirement that the pairing term satisfies Fermi-Dirac statistics implies that there are only six possible pairing matrices Λ_i, listed in the second column of Table I (see, e.g., [33]). As a consequence, starting from h_{SM}, we can obtain six distinct s-wave superconducting states.

The normal state already has broken time-reversal symmetry ($T^2 = -1$); when the superconducting pairing is added these superconductors belong to symmetry class D [2]. We note that our model has a pseudochiral symmetry but its presence is not required for our results. All the models have mirror symmetries $\mathcal{M}_x$, $\mathcal{M}_y$, and $\mathcal{M}_z$, and therefore overall inversion symmetry $\mathcal{I} = \mathcal{M}_x\mathcal{M}_y\mathcal{M}_z$. The representation matrices for the $\mathcal{M}_x$ and $\mathcal{M}_y$ mirror symmetries are shown in Table I, and the matrix for $\mathcal{M}_z$ is the identity matrix. Models $h_{SC,5}$, $h_{SC,6}$, retain C_4 symmetry in the superconducting state with representation matrices given in Table I.

Let us consider the quasiparticle spectra in the weak pairing limit $\Delta_0 < \mu$. Explicitly, we choose $\mu = 1$, $\Delta_0 = 0.5$ and find that models $h_{SC,1}$, $h_{SC,3}$, $h_{SC,6}$ are fully gapped in the bulk by the pairing term while $h_{SC,2}$, $h_{SC,4}$, $h_{SC,5}$ are gapless [see Supplemental Material (SM) [34]]. Model $h_{SC,2}$ ($h_{SC,4}$) has gapless, bulk, quasiparticle states forming a nodal line/loop in the $k_x - k_z$ ($k_y - k_z$) plane, and model h_5 has four nodes in the k_x-k_y plane at k_z values away from any high-symmetry points. We see that models $h_{SC,1}$ and $h_{SC,3}$ have the same symmetry, the same representation for $\mathcal{M}_x$ and
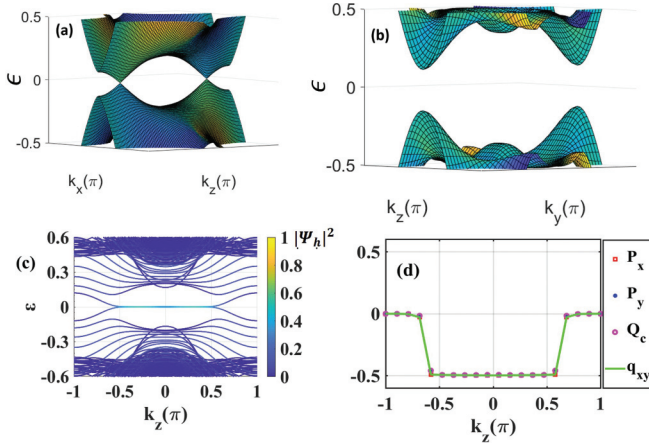
FIG. 2. The surface states of $h_{SC,1}$ in (a) k_x-k_z and (b) k_y-k_z planes. (c) shows the Majorana hinges arc states in the k_z direction. (d) P_x, P_y, Q_c and q_{xy} versus k_z.
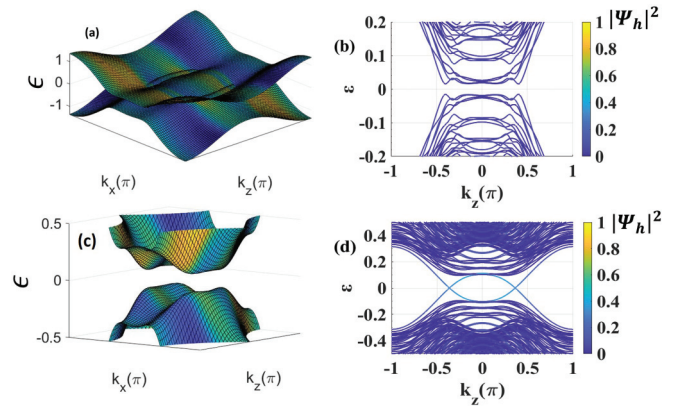

FIG. 3. Model $h_{SC,5}$: Surface states (a) in the k_x-k_z plane, and hinge states (b) along k_z, when $J_z = 0$, (c) and (d), same as (a) and (b), respectively, for the case when $J_z = 0.4$.

$\mathcal{M}_y$, and have the same bulk spectra. Thus, they will have the same essential properties for our study, and henceforth we only consider $h_{SC,1}$. Additionally, models $h_{SC,2}$ and $h_{SC,4}$ are related by a unitary transformation and a C_4 rotation around the z axis so we will only consider $h_{SC,2}$ from now on. While we have focused on particular values of μ and Δ_0, the results do not change qualitatively as long as $\Delta_0 < \mu$, as is appropriate for the weak-pairing limit.

We start by considering model $h_{SC,1}$. The pairing breaks C_4 symmetry, while retaining mirror symmetries, so the bulk are completely gapped [6] (see SM [34] for more details). However, we find that the surfaces $S_{y,\pm}$, perpendicular to the y axis, exhibit two gapless nodes per surface [Fig. 2(a)], whereas the ones perpendicular to the x axis, $S_{x,\pm}$, are completely gapped [Fig. 2(b)]. We then obtain the bands for the hinges and find, as shown in Fig. 2(c), that dispersionless hinge Majorana states are present at the four corners of the xy plane for values of k_z between the two gapless nodes on the S_y surface. In Fig. 2(c) and all the other plots showing the spectrum of hinge states, the color used for each point of the spectrum denotes the magnitude of the square of the corresponding eigenstate at the hinges $|\Psi_h|^2$. These states are reminiscent of the flat bands that appear between the nodes, and at the edges, of a 2D Dirac semimetal.

The structure of the spectrum and symmetry is similar to that of the quadrupolar semimetal obtained in Ref. [32] when $\gamma_i(k_z) \equiv \gamma_i + \chi(k_z)$ [$i = (x, y)$] follow what in Ref. [32] is referred to as path 2, and suggests that the presence of the boundary states, the hinge states in particular, might be due to a second-order topological invariant. To confirm it, we calculated (for details, see SM [34]) the superconducting analog of the quadrupole moment $q_{xy}(k_z)$ for each k_z slice. We have $q_{xy}(k_z) \equiv [P_x(k_z) + P_y(k_z) - Q_c(k_z)]$ mod 1 [6] where $P_x(k_z)$, $P_y(k_z)$ are the surface polarizations in the x and y directions, respectively, and $Q_c(k_z)$ is the corner charge which takes values $1/2$, (0) mod 1, if hinge states are present (absent).

Figure 2(d) shows that $P_x(k_z)$, $P_y(k_z)$ are quantized, and that they take the nontrivial value $-1/2$ for k_z in the interval between the two gapless nodes of the surface states on S_y, the same range of k_z for which we have hinge states. As a

consequence, we find that for values of k_z between the two surface nodes, $q_{xy}(k_z)$ is also nontrivial and therefore that the hinge states in model $h_{SC,1}$ are topologically protected and can be captured by a second-order, quadrupolelike, topological invariant. Interestingly, we find that the presence of the gapless nodes on the surface, and of the hinge states, is not affected by perturbations that break both mirror symmetries, and thus the hinge states are perturbatively stable when the Bogoliubov–de Gennes particle-hole symmetry is maintained even when the mirror symmetry is broken (see SM [34]). Due to the presence of Dirac nodes in the band structure of the surface states, and the finite value of the quadrupolelike invariant we term superconductors like the one described by model $h_{SC,1}$ (and $h_{SC,3}$) as *second-order Dirac superconductors*. This is one of the main results of this work.

For models $h_{SC,2,4}$ the gapless nature of the bulk and surface states leads to obscured hinge modes (see Fig. 2 in SM [34]).

Models $h_{SC,5}$ and $h_{SC,6}$ differ from the previous models in that, in addition to the mirror symmetries $\mathcal{M}_x$ and $\mathcal{M}_y$, they retain the C_4 symmetry of the original semimetal. As mentioned, model $h_{SC,5}$ has nodal points in the bulk quasiparticle spectrum, while $h_{SC,6}$ is fully gapped in the bulk (see SM [34]). We find that both models have gapless surface states but of different nature. Due to the C_4 symmetry, we only show the results for the surface states $S_{y,\pm}$. The surface bands of model $h_{SC,5}$ exhibit two nodal loops [see Fig. 3(a)], whereas the surface bands of model $h_{SC,6}$ exhibit a nodal line at $k_x = 0$ for the S_y surface states ($k_y = 0$ for the S_x surface states), Fig. 4(a). Figures 3(b) and 4(b) show the bands for the hinges for models $h_{SC,5}$ and $h_{SC,6}$ and we see that there are no interesting localized hinge modes present.

However, an external magnetic field can perturb these systems to generate hinge modes. Let us apply a uniform magnetic field, or proximity-couple to a ferromagnet, to generate a Zeeman term $H_z = J_z \tau_3 \sigma_3 \kappa_0$, where J_z is directly proportional to the magnitude of the external magnetic field (we ignore any orbital effects of the magnetic field). This term qualitatively modifies the band structures of $h_{SC,5}$ and $h_{SC,6}$. From Figs. 3(c) and 4(c) we see that the presence of the Zeeman term gaps out the surface states completely
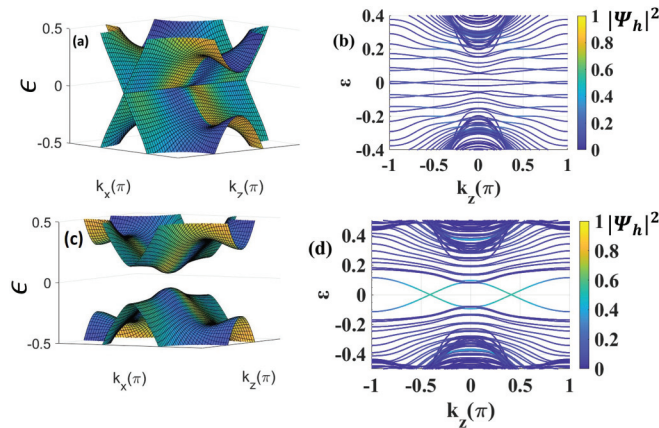
FIG. 4. Model $h_{SC,6}$: Surface states (a) in the k_x-k_z plane, and hinge states (b) along k_z, when $J_z = 0$, (c) and (d), same as (a) and (b), respectively, for the case when $J_z = 0.4$.
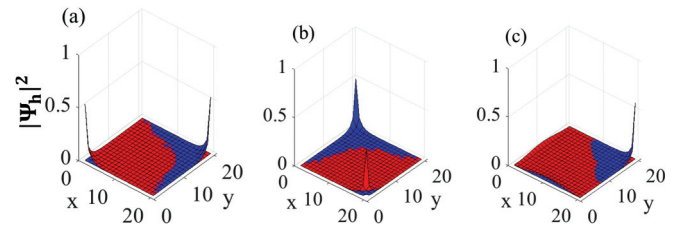

FIG. 5. $|\Psi_h(x, y)|^2$ for model $h_{SC,6}$ in the presence of a Zeeman term. We have two pairs of degenerate states. For each pair $|\Psi_h(x, y)|^2$ is the same. In the figure we show in blue and red the two different $|\Psi_h(x, y)|^2$ profiles. (a) $J_z = 0.4$, $k_z = 0.41\pi$, values for which the helical hinge bands cross [Fig. 4(d)]. (b) $J_z = -0.4$, $k_z = 0.41\pi$. (c) $J_z = 0.4$ plus $C_4\mathcal{M}_x$ breaking perturbation: $0.1\tau_3 r_4^{-1} m_x$. In (c) $k_z = 0.19\pi$, for which we have the lowest positive energy.

(it also gaps out the bulk nodes of $h_{SC,5}$). Furthermore, we see the appearance of clear hinge states within the gap of the surface states, as shown in Figs. 3(d) and 4(d). H_z breaks C_4 symmetry and both mirror symmetries, but leaves the products $C_4\mathcal{M}_x$ (antidiagonal mirror) and $C_4\mathcal{M}_y$ (diagonal mirror) intact. Because of these symmetries, and contrary to the hinge states of the other models discussed in this work, the hinge states of $h_{SC,5}$ and $h_{SC,6}$ (with Zeeman) are: dispersive, nonchiral, and localized only at two of the four hinges related by C_2 symmetry. In addition, we find that the pair of corners where the helical hinge states are localized switches upon a change of sign of the Zeeman term (e.g., switching the direction of the external magnetic field) (see Fig. 5). This phenomenon could be useful for the experimental detection of these systems. We note that magnetic fields were also proposed to induce a HOTSC state in a completely different system with different properties in two dimensions [35].

For $J_z > 0$ ($J_z < 0$) there are two, counterpropagating modes at two of the four corners, and they are $\pm$ eigenstates of $C_4\mathcal{M}_y$ ($C_4\mathcal{M}_x$). The hinge modes are perturbatively stable even in the absence of the two $C_4\mathcal{M}_i$ symmetries as long as particle-hole symmetry is preserved. However, the modes can be destroyed through bulk or surface phase transitions. Because the hinge states are located at opposite sides of the antidiagonal (diagonal), the breaking of the $C_4\mathcal{M}_x$ ($C_4\mathcal{M}_y$) symmetry leads to nonsymmetric hinge states and, for a strong enough $C_4\mathcal{M}_x$ ($C_4\mathcal{M}_y$) symmetry-breaking perturbation, to the almost complete suppression of the hinge states at one corner and the enhancement of the hinge states at the opposite corner, as shown in Fig. 5(c).

In conclusion, we have identified a class of HOTSCs: *second-order Dirac superconductors*. HOTSCs in this class have both topologically protected Dirac cones for states at the surface (d-1 boundary) and topologically protected dispersionless Majorana states at the hinges (d-2 boundary). The coexistence of gapless surface and hinge modes should lead to novel transport properties that would be interesting to compare to those of conventional topological superconductors [2,36–46]. We have then identified 3D superconducting systems that can be driven into a higher-order topological state simply via inclusion of a Zeeman term, having dispersive helical Majorana hinge states that are located at only two (or one) of the corners. We have shown that by varying the relative sign of the Zeeman term and of the mirror-diagonal symmetry-breaking perturbation, the position of the Majorana pairs can be tuned to be at a specific corner, leading to a highly tunable setup for realizing, *and* detecting, helical Majorana states.

[1] R. Resta, Rev. Mod. Phys. **66**, 899 (1994).

[2] C.-K. Chiu, J. C. Y. Teo, A. P. Schnyder, and S. Ryu, Rev. Mod. Phys. **88**, 035005 (2016).

[3] J. Zak, Phys. Rev. Lett. **62**, 2747 (1989).

[4] T. L. Hughes, E. Prodan, and B. A. Bernevig, Phys. Rev. B **83**, 245132 (2011).

[5] A. M. Turner, Y. Zhang, R. S. K. Mong, and A. Vishwanath, Phys. Rev. B **85**, 165120 (2012).

[6] W. A. Benalcazar, B. A. Bernevig, and T. L. Hughes, Science **357**, 61 (2017).

[7] W. A. Benalcazar, B. A. Bernevig, and T. L. Hughes, Phys. Rev. B **96**, 245115 (2017).

[8] F. Schindler, A. M. Cook, M. G. Vergniory, Z. Wang, S. S. P. Parkin, B. A. Bernevig, and T. Neupert, Sci. Adv. **4**, eaat0346 (2018).

[9] Z. Song, Z. Fang, and C. Fang, Phys. Rev. Lett. **119**, 246402 (2017).

[10] F. Schindler, Z. Wang, M. G. Vergniory, A. M. Cook, A. Murani, S. Sengupta, A. Y. Kasumov, R. Deblock, S. Jeon, I. Drozdov, H. Bouchiat, S. Guéron, A. Yazdani, B. A. Bernevig, and T. Neupert, Nat. Phys. **14**, 918 (2018).

[11] M. Ezawa, Phys. Rev. Lett. **120**, 026801 (2018).

[12] M. Ezawa, Phys. Rev. B **98**, 045125 (2018).

[13] J. Noh, W. A. Benalcazar, S. Huang, M. J. Collins, K. P. Chen, T. L. Hughes, and M. C. Rechtsman, Nat. Photonics **12**, 408 (2018).

[14] C. W. Peterson, W. A. Benalcazar, T. L. Hughes, and G. Bahl, Nature (London) **555**, 346 (2018).

[15] S. Imhof, C. Berger, F. Bayer, J. Brehm, L. W. Molenkamp, T. Kiessling, F. Schindler, C. H. Lee, M. Greiter, T. Neupert, and R. Thomale, Nat. Phys. **14**, 925 (2018).

[16] M. Serra-Garcia, V. Peri, R. Süsstrunk, O. R. Bilal, T. Larsen, L. G. Villanueva, and S. D. Huber, Nature (London) **555**, 342 (2018).

[17] M. Ezawa, Sci. Rep. **9**, 5286 (2019).

[18] J. Langbehn, Y. Peng, L. Trifunovic, F. von Oppen, and P. W. Brouwer, Phys. Rev. Lett. **119**, 246401 (2017).

[19] Y. Wang, M. Lin, and T. L. Hughes, Phys. Rev. B **98**, 165144 (2018).

[20] E. Khalaf, Phys. Rev. B **97**, 205136 (2018).

[21] D. Călugăru, V. Juričić, and B. Roy, Phys. Rev. B **99**, 041301(R) (2019).

[22] Z. Wang, B. J. Wieder, J. Li, B. Yan, and B. A. Bernevig, arXiv:1806.11116.

[23] B. J. Wieder and B. A. Bernevig, arXiv:1810.02373.

[24] W. A. Benalcazar, T. Li, and T. H. Hughes, Phys. Rev. B **99**, 245151 (2019).

[25] B. J. Wieder, Z. Wang, J. Cano, X. Dai, L. M. Schoop, B. Bradlyn, and B. A. Bernevig (unpublished).

[26] R.-X. Zhang, W. S. Cole, and S. Das Sarma, Phys. Rev. Lett. **122**, 187001 (2019).

[27] Q. Wang, C.-C. Liu, Y.-M. Lu, and F. Zhang, Phys. Rev. Lett. **121**, 186801 (2018).

[28] Z. Yan, F. Song, and Z. Wang, Phys. Rev. Lett. **121**, 096803 (2018).

[29] C.-H. Hsu, P. Stano, J. Klinovaja, and D. Loss, Phys. Rev. Lett. **121**, 196801 (2018).

[30] Y. Volpez, D. Loss, and J. Klinovaja, Phys. Rev. Lett. **122**, 126402 (2019).

[31] Y.-J. Wu, J. Hou, Y.-M. Li, X.-W. Luo, and C. Zhang, arXiv:1905.08896.

[32] M. Lin and T. L. Hughes, Phys. Rev. B **98**, 241103(R) (2018).

[33] T. Hashimoto, S. Kobayashi, Y. Tanaka, and M. Sato, Phys. Rev. B **94**, 014510 (2016).

[34] See Supplemental Material at http://link.aps.org/supplemental/10.1103/PhysRevB.100.020509 for details on bulk bandstructures, discussion of model $h_{SC,(2)}$, the effect of perturbations on $h_{SC,(1,2)}$ and the calculation of quadrupolelike moment for model $h_{SC,1}$.

[35] X. Zhu, Phys. Rev. B **97**, 205134 (2018).

[36] L. Fu and C. L. Kane, Phys. Rev. Lett. **102**, 216403 (2009).

[37] L. Fu and C. L. Kane, Phys. Rev. B **79**, 161408(R) (2009).

[38] M. S. Foster and E. A. Yuzbashyan, Phys. Rev. Lett. **109**, 246801 (2012).

[39] M. S. Foster, H.-Y. Xie, and Y.-Z. Chou, Phys. Rev. B **89**, 155140 (2014).

[40] Sayed Ali Akbar Ghorashi, S. Davis, and M. S. Foster, Phys. Rev. B **95**, 144503 (2017).

[41] Sayed Ali Akbar Ghorashi, Y. Liao, and M. S. Foster, Phys. Rev. Lett. **121**, 016802 (2018).

[42] B. Roy, Sayed Ali Akbar Ghorashi, M. S. Foster, and A. H. Nevidomskyy, Phys. Rev. B **99**, 054505 (2019).

[43] Sayed Ali Akbar Ghorashi and M. S. Foster, arXiv:1903.11086.

[44] H.-Y. Xie, Y.-Z. Chou, and M. S. Foster, Phys. Rev. B **91**, 024203 (2015).

[45] S. A. Yang, H. Pan, and F. Zhang, Phys. Rev. Lett. **113**, 046401 (2014).

[46] H. Hu, F. Zhang, and C. Zhang, Phys. Rev. Lett. **121**, 185302 (2018).

Supplementary Materials: Second-order Dirac superconductors and magnetic field induced Majorana hinge modes

Sayed Ali Akbar Ghorashi[1], Xiang Hu[1], Taylor L. Hughes[2], Enrico Rossi[1]

[1]*Department of Physics, William & Mary, Williamsburg, Virginia 23187, USA and*

[2]*Department of Physics and Institute for Condensed Matter Theory,*

University of Illinois at Urbana-Champaign, IL 61801, USA

I. BULK SPECTRUM AND CONTINUUM ANALYSIS

We can analyze the bulk quasi-particle spectra by considering the effects of Δ_0 perturbatively on the normal state semimetal by using a continuum $\mathbf{k} \cdot \mathbf{p}$ expansion around the nodes at the two $k_z^{(c)}$. The 16×16 continuum Hamiltonian is

$$
\begin{aligned}
H_{\mathbf{k} \cdot \mathbf{p}, i} = & -\tau_3 \pi_0 \sigma_2 (v k_x \kappa_3 + v k_y \kappa_1) + v_z k_z (\tau_3 \pi_3 \sigma_2 \kappa_2 \\
& - \tau_3 \pi_3 \sigma_1 \kappa_0) - \mu \tau_3 \pi_0 \sigma_0 \kappa_0 - \Delta_0 \tau_2 \pi_1 \Lambda_i
\end{aligned}
\tag{1}
$$

where π_i are Pauli matrices in the valley/node degree of freedom, and v, v_z are velocities ($\hbar = 1$). In the nodal limit $\mu \to 0$, one can determine the nature of the bulk spectra by calculating how the pairing term commutes/anti-commutes with the kinetic terms.

In Fig 1, we present bulk band structures for all the models discussed in this work using the lattice model of Eq. (2) in the manuscript.
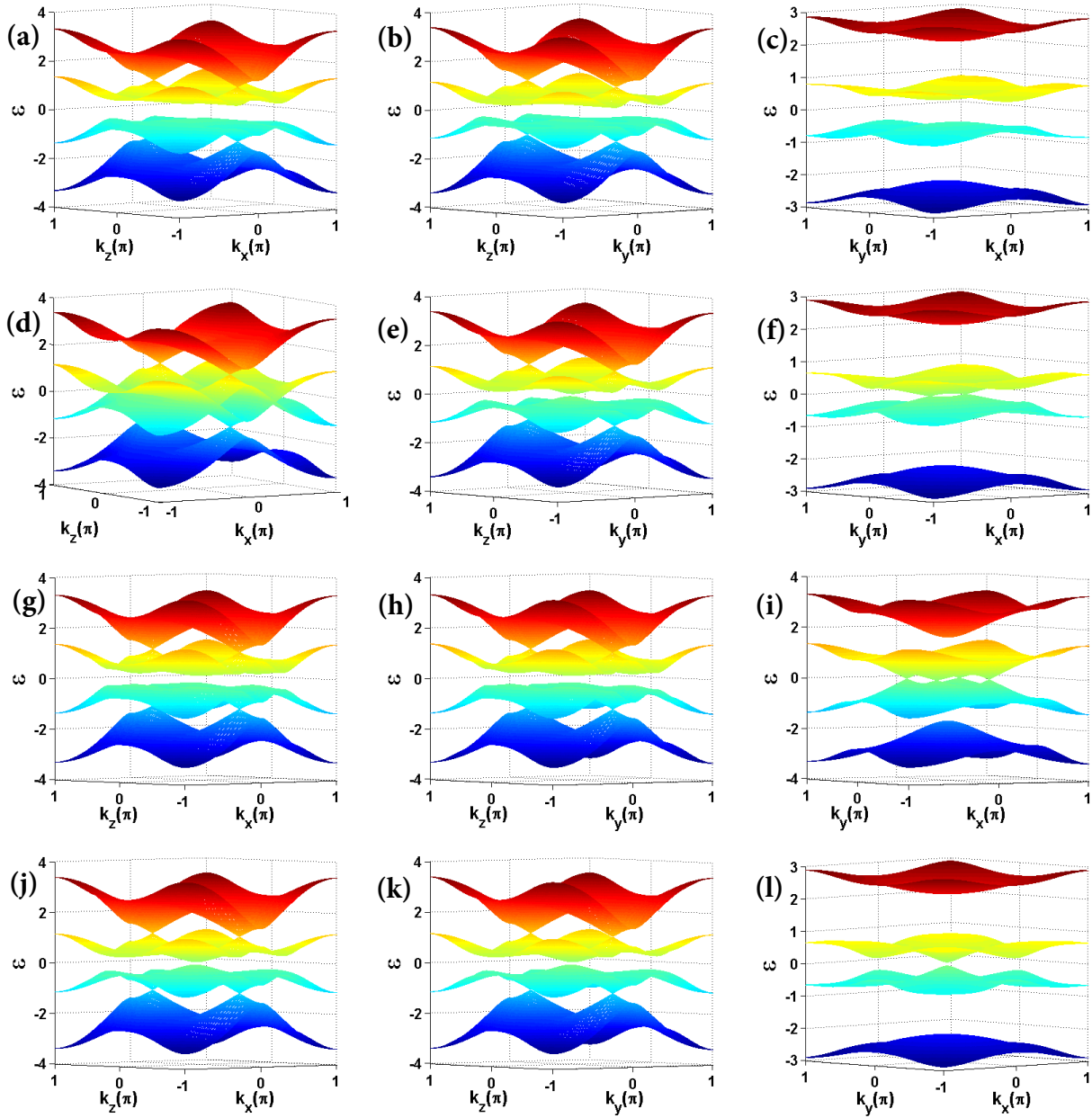
FIG. 1: Bulk spectrum for models $h_{\text{SC},1}, h_{\text{SC},2}, h_{\text{SC},5}$ and $h_{SC,6}$ shown in the first, second, third and fourth rows, respectively. Each row, from left to right, represents $k_x - k_z$ ($k_y = 0$), $k_y - k_z$ ($k_x = 0$) and $k_x - k_y$ ($k_z = 0$ for all model except $h_{SC,5}$ where $k_z = 0.4$ is used) plane.

II.   MODEL $h_{sc,2}$

As mentioned in the manuscript the bulk states of model $h_{\text{SC},2}$. have nodal loops, (see Fig 1), and the surface states are gapless, as shown in Figs. 2 (a), (b). While we do find a small region of localized hinges states in the middle of the spectrum (see Fig. 2 (c)), the gapless bulk and surface states obscure them. It would be difficult to spectroscopically isolate the hinge modes of this model for any practical or experimental purpose. The same is true of model $h_{\text{SC},4}$. Thus, as we noted in the manuscript, while there may be some interesting features of the gapless bulk and surface states of these models left to explore, we leave the study of these models for future works given that in this work our primary interest is in hinge-mode phenomenology.
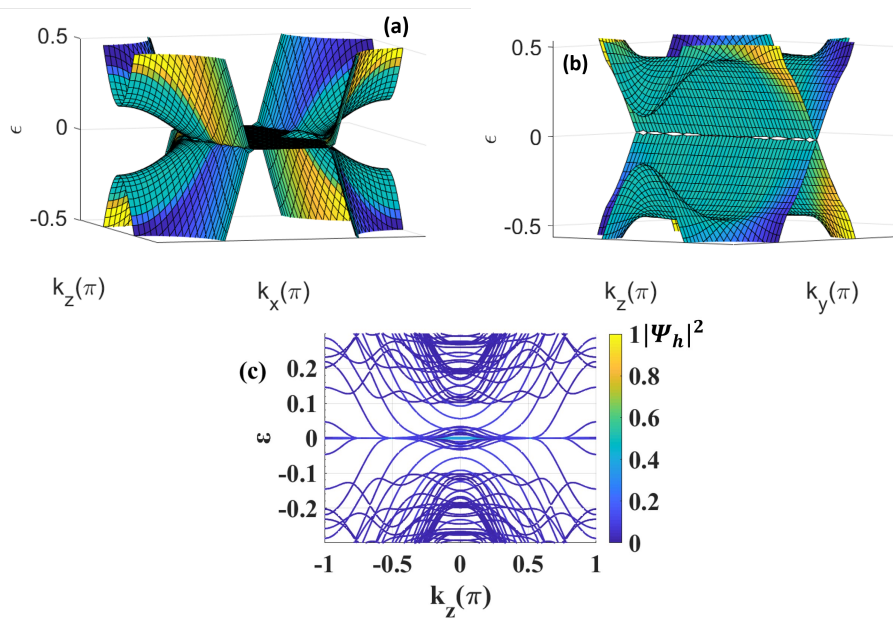
FIG. 2: The surface states of $h_{\mathrm{SC},2}$ in (a) $k_x - k_z$ and (b) $k_y - k_z$ planes. (c) shows the Majorana hinges arc states in k_z direction.

III.   THE EFFECT OF SYMMETRY-BREAKING PERTURBATIONS

In this section we show that the hinges states corresponding to second-order topological superconductors of $h_{\mathrm{SC},1}$ (or $h_{\mathrm{SC},3}$) are robust against mirror-symmetry breaking perturbations, and that the effect of the Zeeman term J_z on the obscured hinges states of models $h_{\mathrm{SC},2}$ (or $h_{\mathrm{SC},4}$).

Figures 3(a) and (b) show the spectrum of hinge states for model $h_{\mathrm{SC},1}$ in the presence of weak $\mathcal{M}_x$ and $\mathcal{M}_y$ breaking perturbations. As is evident hinge states are robust against weak symmetry-breaking perturbations and at most can partially remove degeneracies.
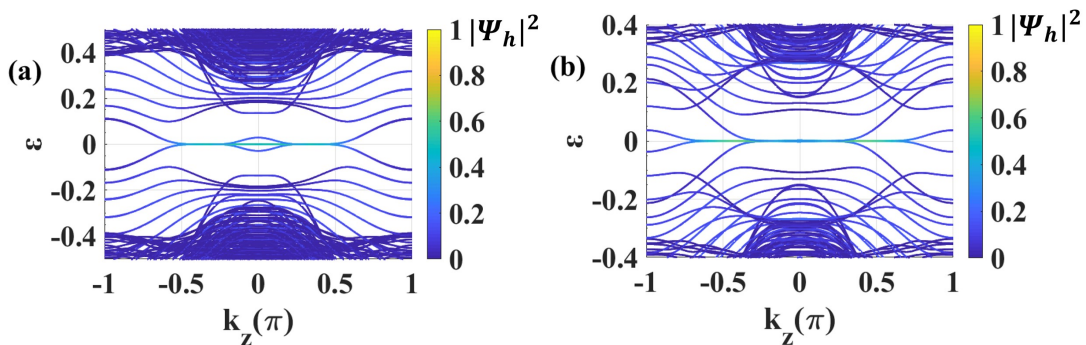

FIG. 3: The hinge states along k_z-direction for $h_{\mathrm{SC},1}$ in the presence of (a) $\mathcal{M}_x$ and (b) $\mathcal{M}_y$ breaking perturbations. $\mu = 1, \Delta_0 = 0.5$ and perturbation strength of 0.1 is used.

Fig. 4, shows the hinge spectrum for model $h_{\mathrm{SC},2}$ in the presence of a magnetic field along the z direction, J_z, for two different values of J_z. We observe that the Zeeman term can only gradually remove some of the gapless points. We could not find any weak perturbation that can fully gap out the hinges states while preserving particle-hole symmetry.
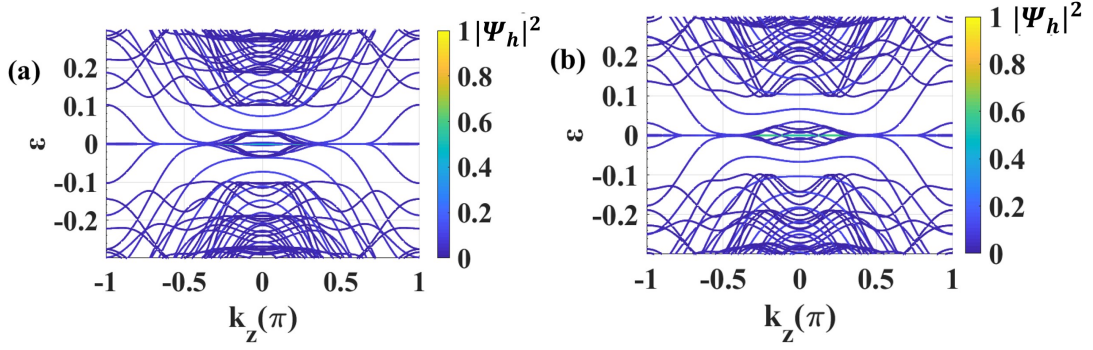
FIG. 4: The hinge states along k_z-direction for $h_{\mathrm{SC},2}$ in the presence of the Zeeman terms with (a) $J_z = 0.4$ and (b) $J_z = 0.6$. $\mu = 1, \Delta_0 = 0.5$ is used.

IV. THE CALCULATION OF THE QUADRUPOLE-LIKE INVARIANT FOR THE SECOND-ORDER DIRAC SUPERCONDUCTORS

For each superconducting Hamiltonian with two orbitals and one spin degree of freedom $H_{\mathrm{SC,i}} = \Psi_{\mathbf{k}}^{\dagger}(\tau_3 h_{\mathrm{SM}}(\mathbf{k}) - \Delta_0 \tau_2 \Lambda_i)\Psi_{\mathbf{k}}$, we can substitute the original basis $\Psi_{\mathbf{k}} = (c_{\mathbf{k}\uparrow}, d_{\mathbf{k}\uparrow}, c_{\mathbf{k}\downarrow}, d_{\mathbf{k}\downarrow}, c_{-\mathbf{k}\uparrow}^{\dagger}, d_{-\mathbf{k}\uparrow}^{\dagger}, c_{-\mathbf{k}\downarrow}^{\dagger}, d_{-\mathbf{k}\downarrow}^{\dagger})^T$ with a new basis $\tilde{\Psi}_{\mathbf{k}} = (c_{\mathbf{k}\uparrow}, d_{\mathbf{k}\uparrow}, c_{\mathbf{k}\downarrow}, d_{\mathbf{k}\downarrow}, \tilde{c}_{\mathbf{k}\uparrow}, \tilde{d}_{\mathbf{k}\uparrow}, \tilde{c}_{\mathbf{k}\downarrow}, \tilde{d}_{\mathbf{k}\downarrow})^T$, where $\tilde{c}$ and $\tilde{d}$ are two additional electron orbitals. Now we have a Hamitonian with the pure electron basis

$$\tilde{H}_i = \sum_{\mathbf{k}} \tilde{\Psi}_{\mathbf{k}}^{\dagger}(\tau_3 h_{\mathrm{SM}}(\mathbf{k}) - \Delta_0 \tau_2 \Lambda_i)\tilde{\Psi}_{\mathbf{k}}. \tag{2}$$

The formulation of the original BdG Hamiltonian in terms of purely electronic degrees of freedom makes direct the connection between the quadrupole moment of non-superconducting systems and the equivalent "quadrupole moment" that can be used to identify higher order topological superconducting states.

The calculation of the polarization and quadrupole for model $h_{\mathrm{SC},1(3)}$ is carried out using the method presented in Ref.[7]. As stated in the main text we have $q_{xy}(k_z) \equiv (P_x(k_z) + P_y(k_z) - Q_c(k_z)) \mod 1$, where q_{xy} is the quadrupole moment, $P_x(k_z), P_y(k_z)$ are the surface polarizations in the x and y directions, respectively, and $Q_c(k_z)$ is the corner charge which takes values $1/2, (0) \mod 1$, if hinge states are present (absent). To obtain the edge-localized polarization $P_x(k_z)$ for a fixed k_z, we place the Hamiltonian $\tilde{H}_{1(3)}(k_z)$ in a geometry which is open in the y direction and periodic in the x direction. We have $P_x = \sum_{R_y=N_y-N_l+1}^{N_y} p_x(R_y)$, where R_y is a site along y in the discretized model, N_y is the size of the system along the y direction (in number of sites of the discretized model), N_l is the finite thickness of the edge layer used in the calculation, and (see Eqs.(5.8) and (5.9) of Ref.[7]):

$$p_x(R_y) = \sum_j \rho^j(R_y)\nu_x^j; \tag{3}$$

where

$$\rho^{j,R_x}(R_y) = \frac{1}{N_x} \sum_{k_x,\alpha} |[u_{k_x}^n]^{R_y,\alpha}[\nu_{k_x}^j]^n|^2, \tag{4}$$

In the equations above j and ν_x^j are the index and eigenvalue for the Wilson loop along k_x, respectively, R_x and R_y are the position in x and y directions. N_x is the size in x direction, $[\nu_{k_x}^j]^n$ represent the $n-$th component of the $j-$th Wannier function, and $[u_{k_x}^n]^{R_y,\alpha}$ is the component of the $n-$th Bloch wave function at R_y with orbital index α. P_y is obtained in a similar way via the substitutions $x \to y$, $y \to x$. We calculate the corner charge using open boundary conditions both in the x and y direction:

$$Q_c = \sum_{R_x=N_x-N_l+1}^{N_x} \sum_{R_y=N_y-N_l+1}^{N_y} \rho(\mathbf{R}), \tag{5}$$

where $\rho(\mathbf{R})$ is the charge density due to the occupied states.

In our calculations, we used $N_x = 50$, $N_y = 50$, $N_z = 19$ and $N_l = 10$. For the bulk Hamiltonian, four bands are occupied. The values of the other parameters are the ones stated in the main text. When calculating the quadrupole moment for model $h_{\text{SC},1}$ we add a small perturbation of the form

$$\delta \tilde{H}_1 = 0.005\tau_0\Gamma_0 + 0.010(\tau_3\sigma_1\kappa_1 + \tau_3\sigma_0\kappa_3). \tag{6}$$

in order to fix the sign of P_x, P_y and Q_c (i.e. to remove the ambiguity due to the fact that these quantities are well definide only up to $\mod 1$).